Inorganic Chemistry

Article

pubs.acs.org/IC

Structure, Bonding, and Phase Relations in $Bi_2Sn_2O_7$ and $Bi_2Ti_2O_7$ Pyrochlores: New Insights from High Pressure and High Temperature Studies

Ashkan Salamat,[†,‡] Andrew L. Hector,[§,*] Paul F. McMillan,[†] and Clemens Ritter[⊥]

[†]Department of Chemistry, University College London, London WC1H 0AJ, U.K.

[‡]European Synchrotron Radiation Facility, BP 220, 38043 Grenoble, Cedex 9, France

[§]School of Chemistry, University of Southampton, Southampton SO17 1BJ, U.K.

[⊥]Institut Laue-Langevin, BP 156, 38042 Grenoble, Cedex 9, France

Supporting Information

ABSTRACT: One of the key points of interest in pyrochlore materials containing bismuth derives from the dielectric properties of some such materials that are linked to the displacements of the bismuth atoms from the ideal site. This study uses high pressure to probe the variations in, and causes of, these displacements. Under compression $Bi_2Ti_2O_7$ does not undergo any phase changes, but $Bi_2Sn_2O_7$ undergoes a similar series of changes to those observed during heating. The trigonal β-$Bi_2Sn_2O_7$ structure is solved from high temperature powder neutron diffraction data and hence the sequence of phases observed in $Bi_2Sn_2O_7$ is discussed for the first time. The variation in Bi displacements can be considered in terms of the frustration of the tetrahedral lattice that accommodates them. It can also be inferred that the main driver for Bi displacement is a deficiency in the bond valence sum of bismuth.

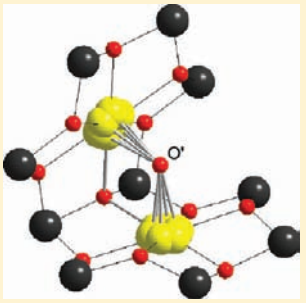

INTRODUCTION

Oxide materials with the pyrochlore structure have many useful properties leading to technological applications, ranging from their use as pigments[1] and catalysts,[2] to frustrated magnetism[3] and superconductivity,[4] and important ferroelectric behavior.[5] Much of the current interest in bismuth-containing pyrochlores stems from their dielectric properties. Compounds in the bismuth zinc niobate (BZN) system have high dielectric constants, low dielectric loss and temperature coefficients of capacitance that are tunable with composition.[6] They also produce near fully dense ceramics upon sintering below 1200 K. Increasingly BZN and related phases are being incorporated into capacitors for microwave applications and thin film devices.[7]

The pyrochlores have general formula $A_2B_2O_7$ where the larger cation A usually belongs to groups 1−3 of the Periodic Table and B is often a transition metal ion. The structure is based on an anion-defective fluorite-type lattice with ordering of the cation sites combined with small displacements relative to the ideal crystallographic positions.[8] The result is normally described in terms of two interpenetrating oxide sublattices with overall composition $A_2B_2O_6O'$. The tungsten bronze-like B_2O_6 component consists of corner sharing BO_6 octahedra that form a three-dimensional network of six-membered rings. The A_2O' network has linear O′−A−O′ bonds and the O′ anions occur in tetrahedral coordination, similar to the arrangement found in cuprite (Cu_2O). The A cation resides within the six-membered rings and forms bonds with the O^{2-} anions, as well as two shorter bonds formed with the O′ anions perpendicular to the ring, resulting in a distorted 8-coordinated site (Figure 1). Typically, pyrochlore structures are formed when the ionic radius ratio of the two cations (A/B) lies between 1.46 and 1.78.[8] In the case of $Bi_2Sn_2O_7$ and $Bi_2Ti_2O_7$ the radius ratios are 1.70 and 1.95, respectively, and hence the value for $Bi_2Ti_2O_7$ lies well outside the usual pyrochlore stability range.[9] This material is unstable at high temperature, decomposing above 743 K with the appearance of an Aurivillius-type $Bi_4Ti_3O_{12}$ phase, and it is typically synthesized *via* sol−gel or co-precipitation routes at low T.[9,10]

Much of the interest in $Bi_2Ti_2O_7$ derives from the Bi^{3+} displacements that occur away from the center of the six-membered rings, that are even larger than those linked to the important dielectric properties of BZN.[6,9] These displacements are usually modeled as a "donut" of statically displaced Bi positions either on the 96*g* or 96*h* Wyckoff sites within space group $Fd\bar{3}m$. Both models result in a hexagonal ring of potential Bi^{3+} sites (Figure 1), with those in 96*h* rotated by 30° in the plane of the ring compared with the 96*g* structure solution. Heat capacity measurements show a residual entropy at low temperature indicating the presence of disorder,[11] and a recent total scattering study of $Bi_2Ti_2O_7$ showed evidence for correlations between neighboring Bi^{3+} site displacements.[12] The term "charge-ice" has been suggested to describe such

Received: April 22, 2011
Published: November 7, 2011

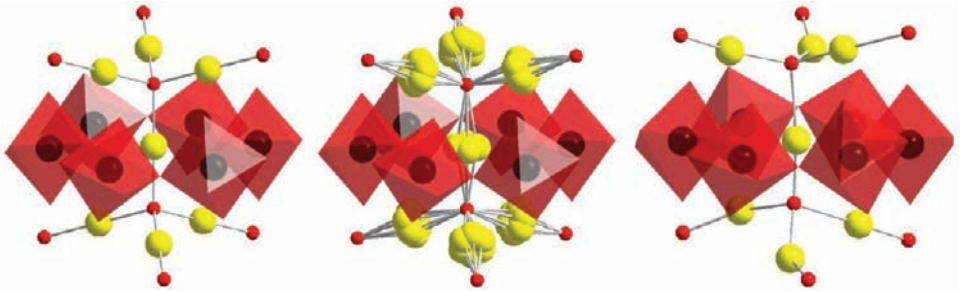

Figure 1. Diagrammatic representation of the A cation environments in a normal cubic pyrochlore such as $La_2Ti_2O_7$ (left), $Bi_2Ti_2O_7$ (center), or α-$Bi_2Sn_2O_7$ (right). Color code: A cation sites in yellow, B cation in black, and O′ in red. O atoms are at the corners of the red octahedra.

frustrated pyroelectric systems,[13] by analogy with the "spin-ice" frustrated magnetic behavior among lanthanide pyrochlores.[3] The displacements are often attributed to the presence of a lone pair associated with the Bi^{3+} ions.[9−13] However, it is not obvious that the Bi^{3+} 6*s* lone pair should necessarily lie off-center and be responsible for the displacements. Alternative models have been discussed in terms of the bond-valence sum at the Bi^{3+} sites.[6,9,14] A recent theoretical study using density functional calculations has suggested that within the ordered domains of the $Bi_2Ti_2O_7$ structure there is no significant off-centering of the lone pair density.[15]

Often correlated Bi^{3+} site displacements can give rise to complex ordered structures with phase transitions occurring between them as a function of temperature. At room temperature, $Bi_2Sn_2O_7$ occurs as the α- polymorph with the noncentrosymmetric monoclinic space group $P1c1$.[16] In this structure, each Bi^{3+} ion is displaced off center within the ring, and also has a displacement along the O′−O′ axis giving rise to long and short Bi−O′ bonds (Figure 1). At 412 K a phase change occurs to a β-$Bi_2Sn_2O_7$ structure with diffraction patterns that can be indexed with a face centered unit cell with its cell edge doubled compared with that of the usual pyrochlore structure (a_o = 21.4 Å),[17] but that has remained unsolved until our present work (see below). Above 903 K a further phase change occurs to a cubic pyrochlore structure (γ-$Bi_2Sn_2O_7$) with statistically averaged Bi^{3+} site displacements analogous to those observed for $Bi_2Ti_2O_7$ at ambient temperature.[18] We recently demonstrated a similar series of phase changes occurring for $Bi_2Hf_2O_7$.[14]

In the present study we applied high pressure techniques to further investigate the structural transformations and to correlate these with the temperature-induced phase changes. The results give important new information on the local bonding constraints that determine the Bi^{3+} cation ordering, related to the relative compressibility of the BiO_8 sites compared with the TiO_6 or SnO_6 coordination environments. Part of the rationale for the study was the idea that compression of the BiO_8 environments could result in either more or less ordered Bi sites and that this could give insights into the relative strengths of lone pair and bond valence sum contributions to Bi displacement. In addition, we carried out a high temperature powder neutron diffraction (PND) and synchrotron X-ray diffraction study in order to resolve the structure of β-$Bi_2Sn_2O_7$.

EXPERIMENTAL SECTION

The $Bi_2Ti_2O_7$ sample was fully characterized during a previous study and its structure was confirmed here by powder X-ray diffraction (PXD, Siemens D5000).[9] $Bi_2Sn_2O_7$ was synthesized according to a literature procedure[16] and checked for composition and purity using PXD and energy dispersive X-ray spectroscopy (Jeol JSM-5910 with Oxford Inca 300). For high pressure experiments the samples were loaded under O_2/H_2O-free conditions into membrane driven diamond anvil cells (DACs) using LiF as a pressure-transmitting medium (PTM). Culet sizes of 300 μm were selected. Rhenium gaskets were preindented to 30 μm with 100 μm holes drilled by electro-erosion and used to contain the samples. Pressures for ambient temperature experiments were determined using ruby fluorescence methods and also from the equation of state for LiF.[19,20] The high temperature data were collected using a resistive heating cell (M7G from DiacellHeliosDAC). It has a stainless steel membrane with an internal ceramic heater. The cell was purged during the heating procedure with a reducing gas mixture (98% Ar/2% H_2) to minimize oxidation of the internal components. X-ray diffraction (XRD) experiments were carried out at beamline I15 of Diamond Light Source (Didcot, UK: λ = 0.44541 Å) at 298 and 623 K and at pressures of up to 60 GPa. XRD patterns were recorded as 2-D angle-dispersive data sets using a MAR image plate. The data were transformed to patterns of intensity versus angle of diffraction and analyzed using the software packages Fit2D,[21] GSAS,[22] FullProf,[23] and PowderCell.[24] Indexing of XRD patterns used the Crysfire[25] package, employing several indexing routines and looking for solutions that were produced by more than one routine and indexed all reflections with a high figure of merit. High temperature synchrotron XRD data (λ = 0.3499 Å) were collected using beamline ID31 at the ESRF, with the capillary of sample heated to 623 K. Powder neutron diffraction (PND) data at 623 K were collected on the D2B diffractometer at the ILL, using λ = 1.5943 Å neutrons, to maximize peak resolution 10′ collimation was employed and only data from the middle of the detector were used.

RESULTS AND DISCUSSION

1. High Pressure Behavior of $Bi_2Ti_2O_7$. The compressional behavior of $Bi_2Ti_2O_7$ was studied by fitting the synchrotron X-ray diffraction data obtained in the DAC using Rietveld analysis. The observed diffraction patterns up to 60 GPa are shown in Figure 2. At low pressure, data could be fitted using the ambient pressure structure[12] with space group $Fd\bar{3}m$ ($a \approx$ 10.40 Å). The Ti and O atoms occupy Wyckoff sites 16*d* and 48*f* at 1/2, 1/2, 1/2 and 1/8, 1/8, 1/8, respectively. The Bi^{3+} ions were placed on 96*h* sites at 0, *y*, −*y* and O′ occupies the 8*a* positions at 1/8, 1/8, *z*. Attempts were made to refine the Bi and O′ positions as a function of pressure, but the data were not sufficient to constrain statistically meaningful solutions. The relative ion positions were then retained at their ambient pressure values throughout the refinements (i.e., *y* = 0.03 and *z* = 0.43, respectively), assuming isotropic thermal parameters. Above 33 GPa the system partially disordered into a fluorite-like phase (Figure 2). Typical Rietveld fits to the data at pressures of 5, 15.5, and 28 GPa are shown in Figure 3, with R_{wp} and R_p ranging from 1.75%, 1.20% to 2.12%, 1.45%, respectively.

dx.doi.org/10.1021/ic200841v | Inorg. Chem. 2011, 50, 11905−11913

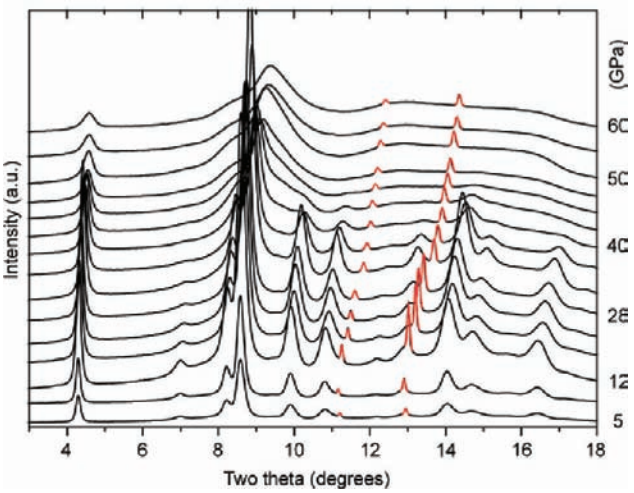

Figure 2. XRD patterns of $Bi_2Ti_2O_7$ during compression from a pressure of 5 to 60 GPa. The sharp reflections at 11.2 and 13.0° at 5 GPa (highlighted in red in the online version) result from LiF used as the pressure transmitting medium.

The compressibility of $Bi_2Ti_2O_7$ pyrochlore was examined by plotting the unit cell volume vs pressure, Figure 4a, and these data highlight the structural stability of this phase until the onset of disordering from 33 GPa. The data were fitted using a Birch–Murnaghan finite strain equation of state (EOS) expanded to third order. The bulk modulus value was refined using a reduced variable F–f plot to give $K_0 = 202 \pm 6.1$ GPa with $K_0' = 2.9 \pm 0.8$ and a best fit V_0 value of 1110 Å^3 (Figure 4b). This was comparable to the unit cell volume determined at ambient conditions using PND (1118 Å^3).[9] Measured bulk moduli of the rare earth pyrochlores are in the range 185–213 GPa.[26]

Above 33 GPa, the diffraction pattern becomes considerably broadened, with main features occurring at around 9.5, 13 and 16° 2θ that could be indexed as the 200, 220, and 222 reflections of a fluorite unit cell with a cell edge near 5.7 Å, and a shoulder to low angle on the 9.5° feature that resembles a fluorite 111 reflection (see Supporting Information, Figure S1). The pyrochlore structure is described as an anion-deficient fluorite structure with cation positions ordered between 6-fold and 8-fold coordinated sites, and a number of studies on lanthanide-group 4 oxide pyrochlores have shown pyrochlore-to-fluorite transitions driven by high temperatures[27] or radiation damage.[28] Attempts to synthesize a pyrochlore of composition $Bi_2Zr_2O_7$ have also previously resulted in a disordered fluorite-type phase with $a_o = 5.39$ Å.[29] The peak observed in pyrochlore at around 4.5° persists through this transformation indicating that disordering is incomplete at 60 GPa, though other pyrochlore peaks are not observable suggesting this is not due to the presence of two distinct phases. This peak would correspond to the 100 reflection of fluorite and could be explained by residual cation ordering that breaks the face centered cubic symmetry of the unit cell. Based on the positions of the 200 reflections, the lattice parameter of the fluorite-like disordered phase varies between 5.60 and 5.53 Å as the pressure is increased from 36 to 60 GPa indicating a highly incompressible structure. The disordered structure was retained following decompression.

2. Ambient Temperature, High Pressure Phase Behavior of $Bi_2Sn_2O_7$. The X-ray diffraction patterns obtained by compressing $Bi_2Sn_2O_7$ to 40 GPa at ambient T

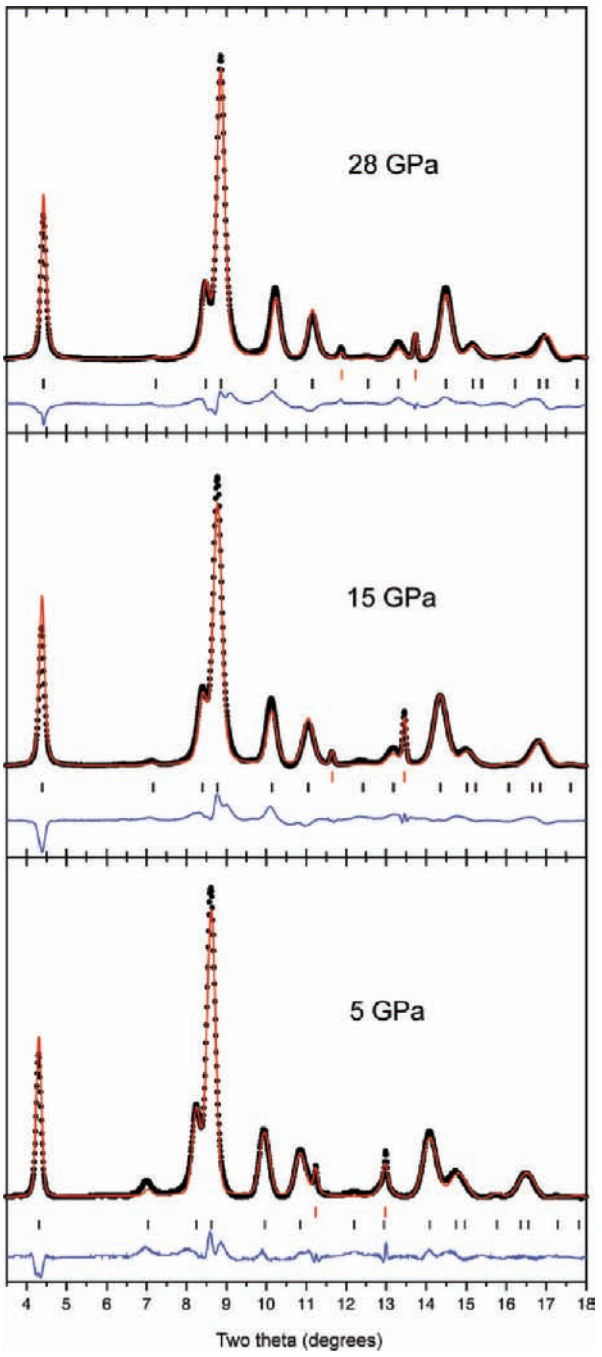

Figure 3. Rietveld fits to XRD patterns of $Bi_2Ti_2O_7$ collected at pressures of 5, 15.5, and 28 GPa in LiF pressure transmitting medium. The data points are shown as (black) crosses and fits as the upper continuous (red) line. The lower continuous line marks the difference. The tick marks show the allowed reflection positions for $Bi_2Ti_2O_7$ (lower, black) and LiF (upper, red).

are shown in Figure 5. Up to 11.6 GPa the structure could be analyzed using the $P1c1$ space group corresponding to the α-$Bi_2Sn_2O_7$ phase that is stable under ambient conditions.[16] Between 13.6 and 20.7 GPa, the observed diffraction pattern closely resembled that of the as-yet unsolved β-$Bi_2Sn_2O_7$ structure that occurs above 413 K at ambient pressure. Above 20.7 GPa, a further transition occurred to a cubic structure with $Fd\bar{3}m$ symmetry that could be correlated with the γ-$Bi_2Sn_2O_7$ polymorph found above 903 K at ambient pressure. Like $Bi_2Ti_2O_7$ this has a standard cubic pyrochlore cell with

dx.doi.org/10.1021/ic200841v | Inorg. Chem. 2011, 50, 11905–11913

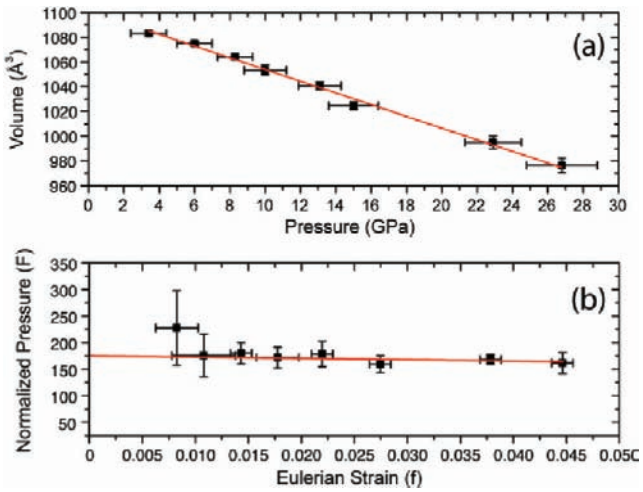

Figure 4. (a) $V(P)$ plot of $Bi_2Ti_2O_7$ during compression from 5 to 33 GPa. (b) Normalized pressure (F) vs the Eulerian strain parameter (f).

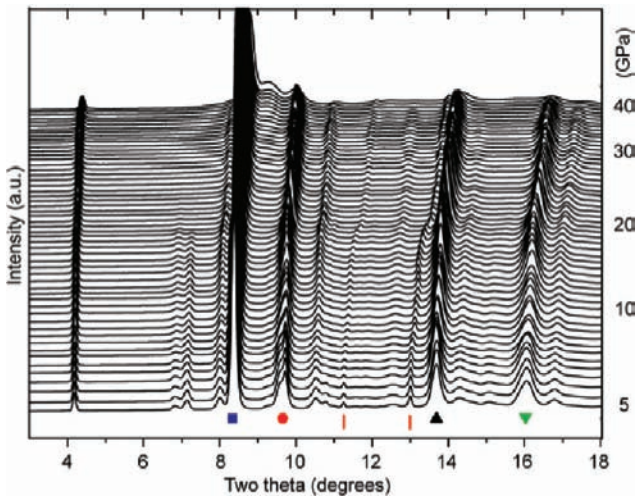

Figure 5. XRD patterns of $Bi_2Sn_2O_7$ during compression from a pressure of 5 (bottom) to 40 (top) GPa. The pressure intervals between the data points are similar in value but not exactly equal. The Bragg peaks with starting positions are marked by vertical ticks (red) are due to reflections from the LiF used as the pressure transmitting medium. Other symbols are relevant to Figure 6 below.

disordered Bi^{3+} displacements.[18] As the pressure was increased beyond 34 GPa, a broad feature emerged around 9° that we attributed to partial cation disordering, as observed for $Bi_2Ti_2O_7$.

The occurrence of the $\alpha-\beta$ transition was marked especially by convergence of the doublet at approximately 9.5° into a single peak, that appeared to be complete by around 11 GPa (Figure 5). A similar disappearance of the multiplet structure was observed for several other reflections. Plots of the full width at half-maximum (FWHM) height of several peaks (Figure 6) clearly suggest that real and significant changes were occurring at the pressures indicated by initial visual inspection of the patterns. Three of the four main peaks exhibited first a slight increase, then a marked decrease up to ~20 GPa, followed by a further increase in their FWHM values on pressure increase. Examination of these plots indicates that the high pressure phase changes occur approximately between 10 and 13 GPa ($\alpha-\beta$), ~20 GPa ($\beta-\gamma$), and ~34 GPa (emergence of the

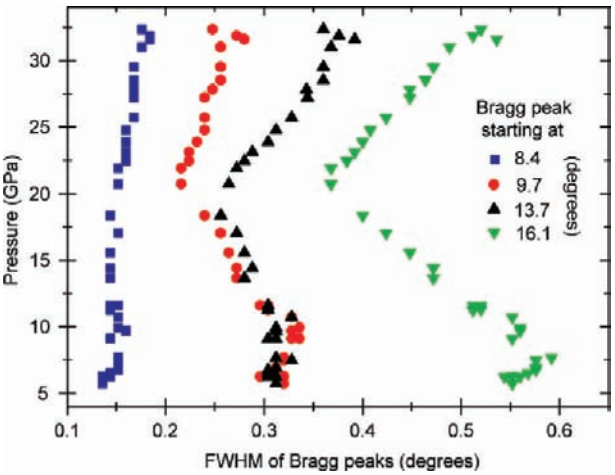

Figure 6. FWHM of the peaks identified in Figure 5 by the same symbols. The 2θ positions of these peaks at ambient pressure are given in the legend.

fluorite-like disordered phase which, as with $Bi_2Ti_2O_7$, is not reversed on decompression).

Data collected for α-$Bi_2Sn_2O_7$ at low pressure were refined using the Rietveld method. The complexity of the structure (176 independent atom positions)[16] and texturing of the diffraction patterns because of the small sample volume precluded detailed refinement of the atom positions. To proceed with our study, the relative atom positions were fixed at their ambient pressure values and only thermal parameters (in four constrained blocks for Bi, Sn, O and O′) and lattice parameters (from a starting point of a = 14.808 Å, b = 14.927 Å, c = 21.383 Å) were refined. The resulting lattice parameters varied from a = 14.881(3) Å, b = 14.924(3) Å, c = 21.451(6) Å and β = 90.0(2)° at 5.7 GPa to a = 14.747(2) Å, b = 14.782(2) Å, c = 21.184(6) Å, and β = 90.1(2)° at 11.6 GPa. Similarly the XRD patterns of the γ-$Bi_2Sn_2O_7$ phase were refined to provide a cubic lattice parameter varying from a_o = 10.385(3) Å at 20.7 GPa to a_o = 10.045(3) Å at 40 GPa. Fits to the data are shown in Figure 7.

Good Le Bail fits were obtained (residuals of R_{wp} = 4.1% and R_p = 2.9%) to the X-ray diffraction data for the β-$Bi_2Sn_2O_7$ phase using either the lattice parameters of α-$Bi_2Sn_2O_7$[16] or a doubled cubic cell as proposed by Kennedy as a starting structure.[17] However, the phase change observed in our data between 11.6−13.6 GPa appears to be real, and no current structure model exists to fit the doubled cubic cell. The best solution that we found from indexing of the XRD data was a hexagonal cell with a = 7.5 Å and c = 37 Å, this had a high figure of merit and allowed us to index all 21 lines used as input. The c-axis of this cell is twice the length of the body diagonal of a standard pyrochlore cell, and hence contains the same number of close packed layers as the doubled cubic cell. Le Bail fits using this hexagonal cell resulted in residuals of R_{wp} = 5.2% and R_p = 3.6%, which were almost indistinguishable from those using the $P1c1$ model of α-$Bi_2Sn_2O_7$ as a starting model. To proceed further with our analysis, we decided to obtain a solution for the structure of the β-$Bi_2Sn_2O_7$ polymorph using diffraction data collected under high temperature conditions.

3. Structure of β-$Bi_2Sn_2O_7$ at 623 K and Ambient Pressure. Synchrotron X-ray and neutron powder diffraction data were collected using samples of $Bi_2Sn_2O_7$ held at 623 K. Le

dx.doi.org/10.1021/ic200841v | Inorg. Chem. 2011, 50, 11905–11913

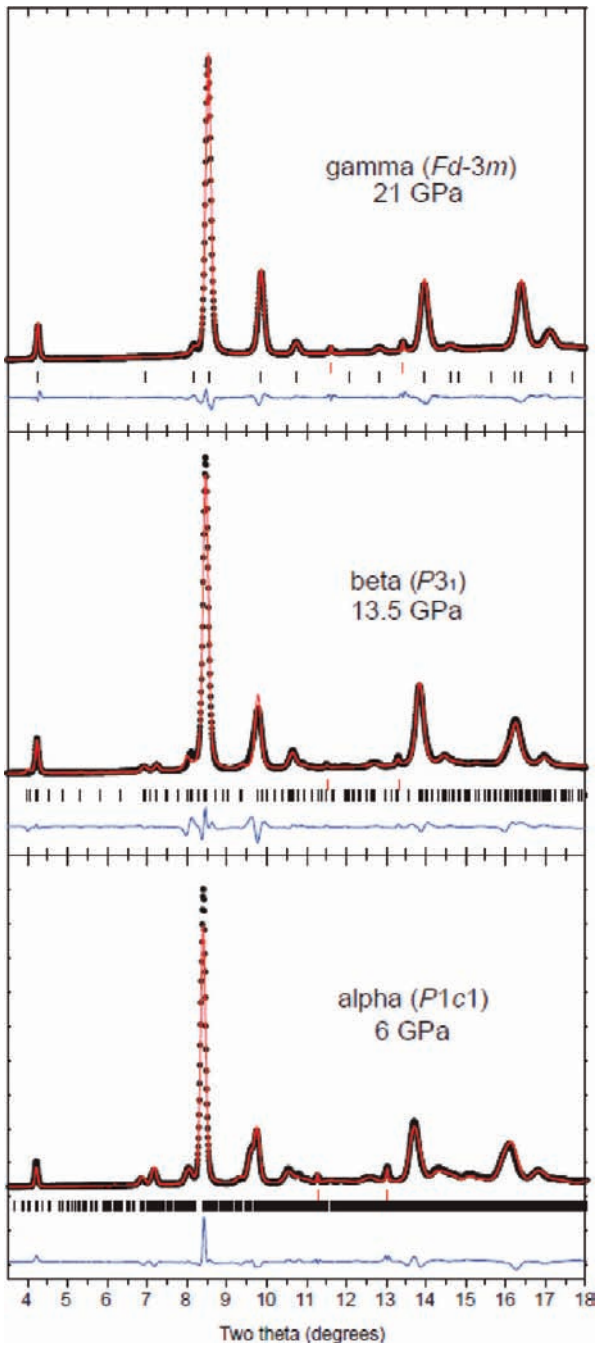

Figure 7. Rietveld fits to XRD patterns of $Bi_2Sn_2O_7$ collected at pressures of 6, 13.5, and 21 GPa in LiF pressure transmitting medium. The data points are shown as (black) crosses and fits to the data as the upper continuous (red) line. The lower continuous line marks the difference plot between the two. The tick marks indicate the allowed reflection positions for the corresponding $Bi_2Ti_2O_7$ phase (lower, black) and LiF (upper, red marks).

Bail refinements in F-43c[14] gave good initial fits with a_o = 21.36 Å. Close inspection of the synchrotron XRD pattern showed a series of weak reflections that were not fitted at 6.68°, 7.66°, 9.32°, 10.39°, 11.97°, and 12.82°. These are all *hhl* reflections with odd Miller indices (see Supporting Information, Figure S2). Inspection of the full set of observed reflections ruled out all body- and face-centered cubic space groups. Although a number of primitive cubic space groups are still plausible, we were unable to generate a suitable cubic structure model and hence investigated the hexagonal cell mentioned above.

The refined value of a_0 was transformed to produce an initial hexagonal cell of a = 7.55 Å, c = 37.01 Å. This cell resembled that of $Ca_{1.89}Ta_{1.86}Sm_{0.16}Ti_{0.1}O_7$ with the 6T-weberite structure in $P3_1$,[30] which is structurally similar to pyrochlore but has a different stacking sequence of the A_3B and AB_3 close packed layers.[31] A series of space group solutions were tried and all trigonal space groups gave acceptable Le Bail fits. However, most of these could be excluded by the need to alternate A_3B and AB_3 layers and thus maintain the basic framework of the pyrochlore structure. Only $P3$, $P3_1$, and $P3_2$ solutions could accommodate this chemical requirement. Initial atom positions were generated from those of $La_2Ti_2O_7$ using the transpose of the inverse of the matrix used to transform the cell parameters,[32] using locally written software,[33] and manually adjusted to reflect symmetry relationships in $P3_1$. The refinement of the PND data using this model proceeded smoothly, though the large number of unconstrained atom positions resulted in the need to strongly damp changes in their positions and to constrain isotropic thermal displacement parameters to a single value for each atom type (Bi, Sn, O, O′). A best fit was obtained with R_{wp} = 5.86%, R_p = 4.47%, R_{F2} = 6.34%, 135 positional parameters from 132 resolved reflections, and lattice parameters of a = 7.58033(8) Å and c = 37.1321(7) Å. A fitted PND pattern is shown in Figure 8 and full structure details, including atom positions, are available as Supporting Information.

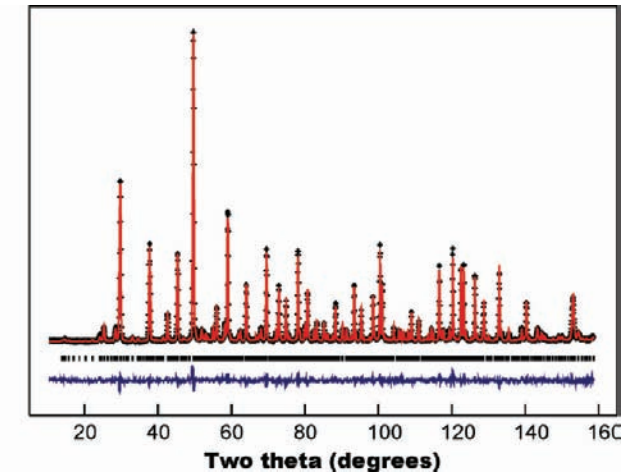

Figure 8. Rietveld fit to the PND pattern of $Bi_2Sn_2O_7$ at 623 K. The data points are shown as crosses, the fit as the upper continuous (red) line and the lower continuous (blue) line the difference. Tick marks show the allowed reflection positions for the $P3_1$ β-$Bi_2Sn_2O_7$ structure. Zoomed regions of this fit are available as Supporting Information (Figure S3).

The resulting structure of β-$Bi_2Sn_2O_7$ is shown in Figure 9. It is closely related to that of cubic pyrochlore, with the key difference being a doubling of the stacking sequence of the cubic close packed layers such that the unit cell contains 6 layers of $Bi_4Sn_4O_{12}O'_2$ units. The volume is 1847.803(12) Å^3, that is, 1.5 times that of a standard cubic pyrochlore cell, and the cell is metrically cubic with $\{\sqrt{2}a/(c/2\sqrt{3})\}$ = 1.0001(3).

The SnO_6 octahedra in this β-$Bi_2Sn_2O_7$ structure are quite regular, with an average Sn−O distance of 2.07 Å. At ambient

dx.doi.org/10.1021/ic200841v | Inorg. Chem. 2011, 50, 11905–11913

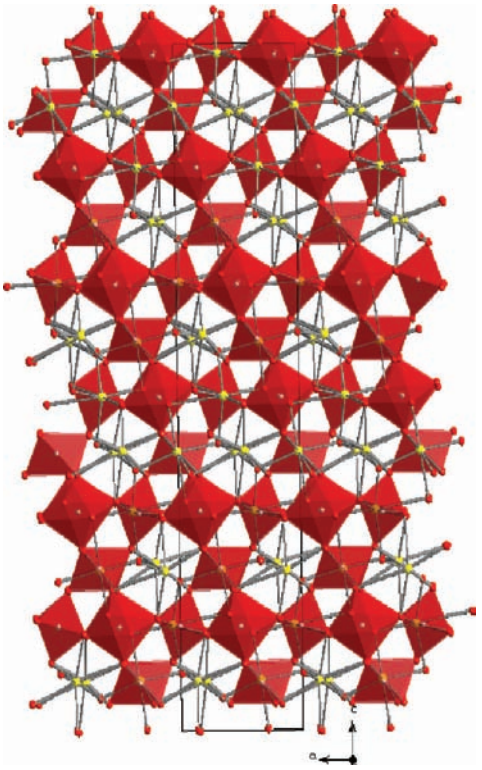

Figure 9. Structure of β-$Bi_2Sn_2O_7$ viewed along [010] (50% probability ellipsoids) with SnO_6 units shown as (red) octahedra and Bi atoms in yellow.

temperature α-$Bi_2Sn_2O_7$ has an average Sn−O distance of 2.054 Å[16] (BVS = 3.9(3)) and in γ-$Bi_2Sn_2O_7$ at 998 K this distance is 2.066 Å. The local distortion of the $BiO_6O'_2$ sites that is seen in α- and γ-$Bi_2Sn_2O_7$ (disordered in the latter) is also observed here. The average O′−Bi−O′ angle is 161°, similar to values obtained in the α- (162° average) and γ- (162.5°) polymorphs. Unfortunately the large number (44) of independent atom positions resulted in relatively high uncertainties in the atom positions from this powder diffraction study and there is some variation in the shapes of the coordination spheres, e.g. O′−Bi−O′ varied from 154.4(25) (Bi4) to 168.1(19) Å (Bi1). There are similar problems with the published structure of α-$Bi_2Sn_2O_7$,[16] where O′−Bi−O′ values are between 136.1 and 178.7°. Ultimately a single crystal study will be required to provide the resolution to fully understand the Bi site displacements in both these phases (if a suitable sample can be prepared). Nonetheless the eight Bi coordination environments all have similar shapes, Figure 10, with the Bi strongly displaced from the center of the puckered ring of 6 O atoms. The average displacement across the ring is 0.42 Å, a similar value to the average displacement in α-$Bi_2Sn_2O_7$ of 0.44 Å.[16] On average the displacement along the O′−O′ axis is 0.08 Å but typically the Bi−O′ distances were within esd and the presence of a displacement in this direction is not proven. The average bond-valence sum at the Bi atoms is 2.8(3).

The structure solution for β-$Bi_2Sn_2O_7$ described above was then applied to the ambient temperature, high pressure XRD data (Rietveld fits with fixed atom positions). Lattice parameters varied from a = 7.385(1) Å and c = 36.298(8) Å at 13.6 GPa, to a = 7.359(2) Å and c = 36.215(9) Å at 18.4 GPa.

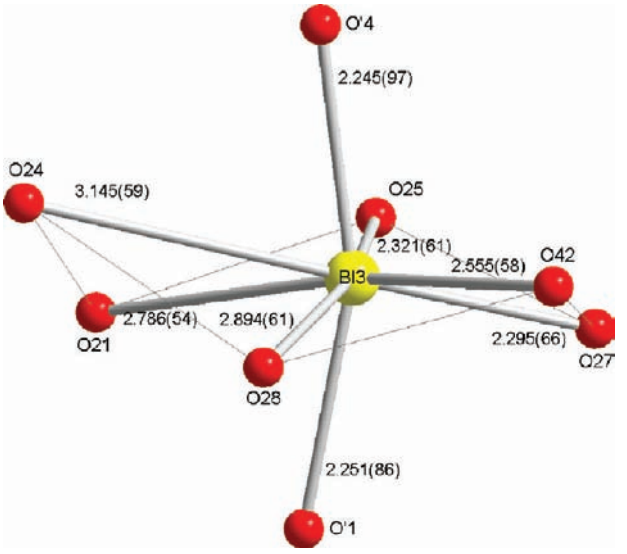

Figure 10. Coordination environment around Bi3, showing the puckered ring of six O atoms and the O′ atoms above and below.

4. High-Pressure Phase Behavior of $Bi_2Sn_2O_7$ at T = 623 K. In order to further link the structural transformations and polymorphic phase behavior of $Bi_2Sn_2O_7$ at high pressure and high temperature, we collected X-ray diffraction data in the resistively heated DAC at T = 623 K at pressures between 1 and 40 GPa (Figure 11). At this temperature the β-$Bi_2Sn_2O_7$ phase

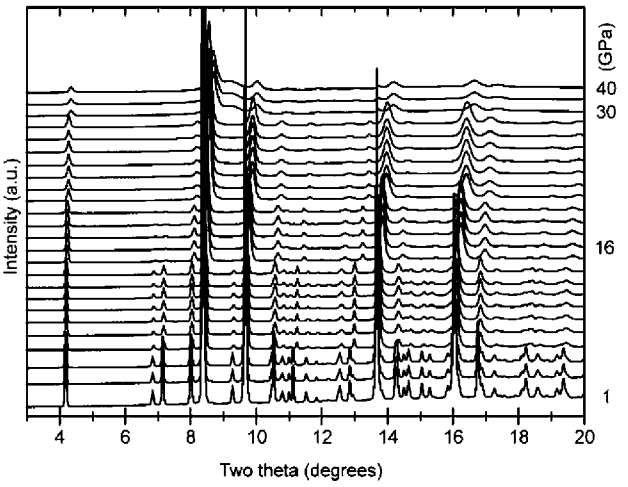

Figure 11. XRD patterns of $Bi_2Sn_2O_7$ during compression at 623 K from a pressure of 1 (bottom) to 40 (top) GPa. The pressure intervals are similar in value but not equal.

is found at ambient pressure and compression results in a phase change to the γ-$Bi_2Sn_2O_7$ structure type at 16 GPa. Lattice parameters varied from a = 7.498(1) Å, c = 36.885(9) Å at 1 GPa to a = 7.370(1) Å, c = 36.750(9) Å at 16 GPa. Similarly the XRD patterns of the γ-$Bi_2Sn_2O_7$ were refined with the lattice parameter varying from a = 10.427(2) Å at 20 GPa to a = 10.168(3) Å at 40 GPa.

5. Discussion of the Differences between the α-, β-, and γ-$Bi_2Sn_2O_7$ Structures. Fairly regular SnO_6 octahedra with similar Sn−O distances are found in all three polymorphs of $Bi_2Sn_2O_7$ and it is clear that the Bi−O′ sub lattice is the part of the structure that undergoes the greatest change. In α-

dx.doi.org/10.1021/ic200841v | Inorg. Chem. 2011, 50, 11905–11913

$Bi_2Sn_2O_7$ the Bi^{3+} ions are displaced away from the center of the puckered ring of O atoms and also toward one of the O′ atoms (Figure 1).[16] Despite uncertainties in the precise shapes of the Bi coordination spheres due to the limitations of the data refinements from the powder diffraction studies, the average difference between the two Bi−O′ distances associated with the 32 Bi atoms is approximately 0.34 Å, and a consistent ice-like pattern of two longer and two shorter bonds within each O′Bi_4 tetrahedron is apparent. Such a pattern cannot be identified in the β-$Bi_2Sn_2O_7$ data. The average difference between the two Bi−O′ distances of the eight Bi atoms is 0.15 Å, and in most cases the displacement is within one estimated standard deviation (esd) from the refined data. Hence the main displacement in β-$Bi_2Sn_2O_7$ seems to be that within the BiO_6 puckered ring. In γ-$Bi_2Sn_2O_7$ a similar displacement within the puckered ring is also observed, but this results in a disordered pattern of Bi^{3+} site occupancies, and hence to a donut-like ring.[18] In $Bi_2Ti_2O_7$ (Figure 1), which is isostructural with γ-$Bi_2Sn_2O_7$, short-range correlations between the Bi displacements in adjacent cells have been observed.[12]

The A−O′ sub lattice in pyrochlores forms a tetrahedral network with the O′ atoms arranged in a diamond-like lattice and the A cations at the centers of the O′−A−O′ bonds. A displacement of Bi within the puckered ring as observed for β- and γ-$Bi_2Sn_2O_7$ is locally analogous to that of O^{2-} ions within the β-cristobalite (SiO_2) structure.[34] There are three main interactions between Bi sites that need to be considered in the context of any correlated displacements (Figure 12), these are

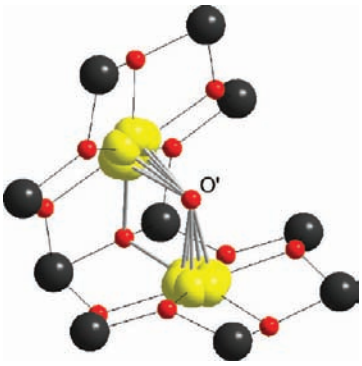

Figure 12. Connectivity between neighboring Bi centers in γ-$Bi_2Sn_2O_7$ via O′ or O, showing the six disordered positions of the Bi atoms (yellow) surrounded by linked puckered Sn_6O_6 rings (Sn atoms black, O atoms red).

through-space electrostatic repulsions, interactions through the bridging O atom at the shared corner between two of the SnO_6 octahedra (i.e., bond valence sum (BVS) considerations), and interactions through the tetrahedral O′ atom (also BVS-related). The first two would mainly result in correlations between displacements within the puckered ring: if one Bi atom is displaced toward the O atom then there will be a tendency for the other to be displaced away from it. Any displacement out of the puckered ring, toward O′, would result in an increase in the BVS of O′ and a reduction in that of the O′ on the other side of the Bi atom. This displacement will tend to lead toward an ice-like arrangement of two long and two short bonds around each O′ as seen in α-$Bi_2Sn_2O_7$. Within the tetrahedral network, both types of interaction would be expected to involve some geometrical frustration as encountered in ice-like structures such as spin-ice pyrochlores that have received recent attention for their dynamic behavior, reported to constitute a new phenomenon termed "magnetricity".[3]

Bismuth displacements in pyrochlores are typically discussed in terms of accommodating either an active lone pair or the BVS of the Bi^{3+} cation. Whatever the driving force for Bi^{3+} displacements, it is clear that the α-$Bi_2Sn_2O_7$ phase has a combination of interactions that lead to ordered displacements both within and out of the puckered ring. In β-$Bi_2Sn_2O_7$, the displacements out of the puckered ring are not observed. It appears that as the temperature is increased the correlation length of any displacement out of the ring has become too short to be observed by diffraction and thus this interaction is weaker or more frustrated than that within the puckered ring. If this is the case a single crystal study of β-$Bi_2Sn_2O_7$ could show extension of Bi ellipsoids perpendicular to the ring. As the temperature increases further the correlation length of the displacement within the ring is also reduced, and the displacement fluctuations become disordered. The effect of these phase changes is to increase the average symmetry of the crystal structures with increasing temperature (more symmetrical space groups), although on examination of the disorder at the Bi sites the expected increase in entropy with temperature is apparent.

6. Discussion of the High Pressure Phase Behavior of $Bi_2Ti_2O_7$ and $Bi_2Sn_2O_7$. $Bi_2Ti_2O_7$ adopts a disordered cubic pyrochlore structure at ambient temperature and pressure that is also observed for γ-$Bi_2Sn_2O_7$ above 903 K or above 20 GPa at 298 K. This structure does not undergo transitions to more ordered Bi site positions as the pressure is increased. The only effect of pressurization was to cause reductions in cell volume and ultimately partial cation disordering toward a fluorite-like phase. It is noteworthy that $Bi_2Ti_2O_7$ does not undergo any phase changes on cooling to 2 K.[9]

Either heating α-$Bi_2Sn_2O_7$, the ambient temperature/pressure polymorph of this material, or subjecting it to elevated pressures at ambient pressure, results in apparently analogous series of phase transitions. The volumes obtained on compression at room temperature and at 623 K are compared in Figure 13, scaled to the unit cell volume of the γ-$Bi_2Sn_2O_7$

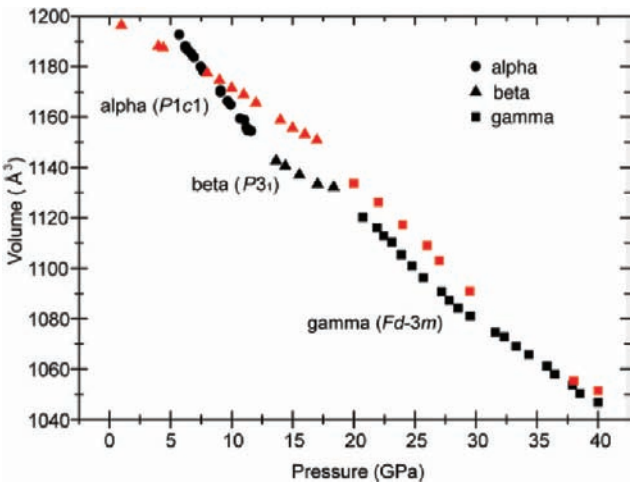

Figure 13. Variation in the volume of $Bi_2Sn_2O_7$ during isothermal compression at 298 K (black symbols) and 623 K (red symbols). The volumes have been normalized to that of a "normal" (i.e., cubic with $a_o \approx 10$ Å) pyrochlore structure by dividing the α-$Bi_2Sn_2O_7$ volumes by 4 and the β-$Bi_2Sn_2O_7$ volumes by 1.5.

dx.doi.org/10.1021/ic200841v | Inorg. Chem. 2011, 50, 11905–11913

phase. At ambient temperature the $\alpha-\beta$ and $\beta-\gamma$ transitions are clearly marked by discontinuities occurring between 11.6 − 13.6 GPa and 18.4 − 20.7 GPa, respectively. At 623 K, the $\beta-\gamma$ transition appears to have shifted to slightly lower pressure, approximately 16 GPa. The slope of the V(P) plot is clearly different for the three polymorphs, but is notably similar for the β- and γ-$Bi_2Sn_2O_7$ phase transitions at the two different temperatures examined in our high-P,T studies. The $\beta-\gamma$ transition and the cation disordering above 34 GPa are marked by apparently unphysical upward changes in curvature near the transition pressures, but these are likely due to errors in analysis of the unit cell parameters obtained during the single phase refinements when both phases are actually present. It is notable that the V(P) relation of $Bi_2Sn_2O_7$ in the high temperature data set crosses that for obtained at ambient T, consistent with the negative ΔV observed in the α- to β-$Bi_2Sn_2O_7$ transition at ambient pressure.[16] Figure 14 summarizes our current knowledge of the P,T phase relations within the $Bi_2Sn_2O_7$ system.

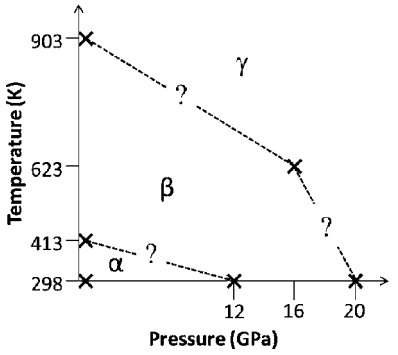

Figure 14. Phase diagram of $Bi_2Sn_2O_7$ summarizing the temperatures and pressures of phase transitions observed in this study and in previous work.[16−18]

During their measurements of cell volume versus temperature at ambient pressure, Evans et al. noted the $\alpha-\beta$ and $\beta-\gamma$ transitions to occur at 410 and 900 K, respectively, with a negative volume change in each case. In the case of the $\alpha-\beta$ transition, we estimate ΔV from the published data[16] as −5 Å^3 relative to the $P1c1$ cell of the α-$Bi_2Sn_2O_7$ phase or $\Delta V = -1.9 \times 10^{-7}$ m^3 per mole of $Bi_2Sn_2O_7$. The volume change associated with the $\beta-\gamma$ transition appears to be of the same order. The variation of the transition temperature with pressure is governed by the Clausius−Clapeyron equation:

$$dT/dP = \Delta V/\Delta S$$

Both the $\alpha-\beta$ and $\beta-\gamma$ transitions are likely to be associated with positive changes in the entropy, as increased disorder in the O^{2-} and Bi^{3+} ion positions is encountered in the sequence $\alpha-\beta-\gamma$, and there may be enhanced vibrational entropy as lower frequency modes appear at lower energies for the high pressure polymorphs.[35] The result is that we expect a negative Clapeyron slope to occur for both the $\alpha-\beta$ and $\beta-\gamma$ transitions, consistent with the suggestion that the structural transformations observed in our study at high pressure are linked to the $\alpha-\beta-\gamma$ transitions recorded at ambient P and high T.

We also obtained data on $Bi_2Sn_2O_7$ transitions at high pressure and at T = 623 K. Extrapolating our ambient temperature results in Figure 13 to ambient pressure we estimate a much larger negative volume change for the $\alpha-\beta$ transition, on the order of $\Delta V = -63$ Å^3 relative to the standard pyrochlore unit cell used in Figure 13, or -1.9×10^{-5} m^3 mol^{-1}. That result suggests that the entropy change for the $\alpha-\beta$ transition at ambient pressure and high temperature is quite different to that at high pressure and ambient temperature. The situation is similar for the $\beta-\gamma$ transition, where we have observed a decrease in the phase transformation pressure with increased temperature as expected (Figure 14). However, the large change in the dT/dP slope either indicates a rapid change in the ΔS value as the P,T conditions are changed, or that the two transitions might not be linked directly: in that case, there could exist a further phase transition between $\gamma-\gamma'$ polymorphs within the system under high-P,T conditions.

This high pressure study was initially conceived to explore the effects of pressure on $Bi_2Ti_2O_7$ and $Bi_2Sn_2O_7$ to investigate the relative effects of Bi^{3+} lone pairs vs bond valence sum deficiencies in the structural distortions that are related to the dielectric properties. We surmised that application of pressure would compress the $BiO_6O'_2$ coordination sphere more rapidly than the more rigid SnO_6 sites. Such differential site compression would

(i) Restrict space for the lone pair on the Bi^{3+} cation. If lone pair effects were the cause of Bi displacement, those displacements would be increased by the application of pressure that would compress the Bi coordination sphere and hence restrict space for the lone pair. Hence the disordered pyrochlore phase ($Bi_2Ti_2O_7$) would become more ordered.

(ii) Decrease the need for Bi^{3+} site distortions to satisfy the local bonding requirements. If BVS (Bi underbonding) effects were the dominant cause of the structural distortion, compression would decrease the need for off-center Bi displacements to satisfy the bonding requirements of the central atom. Hence the ordered pyrochlore phase ($Bi_2Sn_2O_7$) would become more disordered with increasing pressure.

These arguments are most compelling when considering the α- to β-$Bi_2Sn_2O_7$ transition, involving the Bi^{3+} ions moving into the plane of the puckered ring, than for the $\beta-\gamma$ transition where the lack of refined atom positions from the high pressure data precludes detailed assessment of the space around Bi. However, the experimental findings do support the idea that under compression the BVS is more significant than any lone pair effects in these insulating dielectric bismuth pyrochlore phases.

CONCLUSIONS

Compression of $Bi_2Ti_2O_7$ does not result in any phase changes until around 33 GPa, when the structure collapses toward a disordered fluorite-type lattice. $Bi_2Sn_2O_7$ undergoes the same series of phase transitions on compression as on heating, from the monoclinic α-$Bi_2Sn_2O_7$ structure to trigonal β-$Bi_2Sn_2O_7$ between 11.6 and 13.6 GPa and then to the cubic γ-$Bi_2Sn_2O_7$ between 18.4 and 20.7 GPa. The fluorite phase starts to appear around 34 GPa. The trigonal β-$Bi_2Sn_2O_7$ structure contains 12 formula units in a cell that has a doubled stacking sequence of the close packed layers compared with a standard pyrochlore. It has a similar bismuth site displacement to that found in γ-$Bi_2Sn_2O_7$ except that it exhibits long-range order. No evidence was found for a displacement out of the plane of the puckered ring of oxygen positions as exhibited in α-$Bi_2Sn_2O_7$. On heating

dx.doi.org/10.1021/ic200841v | Inorg. Chem. 2011, 50, 11905−11913

the α- to β- to γ-$Bi_2Sn_2O_7$ phase transitions can be considered in terms of the frustration inherent to the tetrahedral network which causes progressive disordering. The observation that the same series of transitions occurs with the application of pressure suggests that the reduced bond valence sum at bismuth is a key driver for Bi displacement from the ideal site in the pyrochlore structure.

■ ASSOCIATED CONTENT

Supporting Information

Full crystallographic data for β-$Bi_2Sn_2O_7$ in cif format plus further refinement details and BVS values. This material is available free of charge via the Internet at http://pubs.acs.org.

■ AUTHOR INFORMATION

Corresponding Author

*E-mail: a.l.hector@soton.ac.uk.

■ ACKNOWLEDGMENTS

We would like to thank Diamond Light Source for the award of beam time on I15 (EE694), Dr. Monica Amboage for helping with the beamline, ILL for time on D2B, and Simon Kimber and Adrian Hill (ESRF) for collecting high T data on ID31. We gratefully acknowledge Mike Webster for help with the cell transformations, Pietro Chirico, Rachael Hazael Mitchell and Katherine Woodhead for assisting in data collection and Paul Boxley for automating data analysis. P.F.M. and A.S. thank EPSRC for support under an EPSRC Senior Research Fellowship (EP/D07357X/1).

■ REFERENCES

(1) Weller, M. T.; Hughes, R. W.; Rooke, J.; Knee, C. S.; Reading, J. *Dalton Trans.* **2004**, 3032.

(2) (a) Felthouse, T. R. *J. Am. Chem. Soc.* **1987**, *109*, 7566. (b) Van Veen, J. A. R.; Van Der Eijk, J. M.; De Ruiter, R.; Huizinga, S. *Electrochim. Acta* **1988**, *33*, 51. (c) Abe, R.; Higashi, M.; Zou, Z.; Sayama, K.; Abe, Y. *Chem. Lett.* **2004**, *33*, 954.

(3) (a) Bramwell, S. T.; Gingras, M. J. P. *Science* **2001**, *294*, 1495. (b) Greedan, J. E.; Raju, N. P.; Maignan, A.; Simon, Ch.; Pedersen, J. S.; Niraimathi, A. N.; Melin, E. G.; Subramanian, M. A. *Phys. Rev. B* **1996**, *54*, 7189.

(4) (a) Hanawa, M.; Muraoka, Y.; Tayama, T.; Sakakibara, T.; Yamamura, J.; Hiroi, Z. *Phys. Rev. Lett.* **2001**, *87*, 187001. (b) Yonezawa, S.; Muraoka, Y.; Matsushita, Y.; Hiroi, Z. *J. Phys.: Cond. Matt.* **2004**, *16*, L9.

(5) Bernard, D.; Pannetier, J.; Lucas, J. *Ferroelectrics* **1978**, *21*, 429.

(6) Levin, I.; Amos, T. G.; Nino, J. C.; Vanderah, T. A.; Rendall, C. A.; Lanagan, M. T. *J. Solid State Chem.* **2002**, *168*, 69.

(7) (a) Ren, W.; Trolier-McKinstry, S.; Randall, C. A.; Shrout, T. R. *J. Appl. Phys.* **2001**, *89*, 767. (b) Lee, Y. C.; Hong, Y. P.; Kim, D. M.; Ko, K. H. *Electron. Lett.* **2006**, *42*, 851. (c) Park, J.-Y.; Xian, C.-J.; Seong, N.-J.; Yoon, S. G.; Son, S. H.; Chung, H.-M.; Moon, J.-S.; Jin, H.-J.; Lee, S.-E.; Lee, J.-W.; Kang, H.-D.; Chung, Y.-K.; Oh, Y.-S. *Microelectronics Reliability* **2007**, *47*, 755.

(8) Subramanian, M. A.; Aravamudan, G.; Subba Rao, G. B. *Prog. Solid State Chem.* **1983**, *15*, 55.

(9) Hector, A. L.; Wiggin, S. B. *J. Solid State Chem.* **2004**, *177*, 139.

(10) (a) Radosavljevic, I.; Evans, J. S. O.; Sleight, A. W. *J. Solid State Chem.* **1998**, *136*, 63. (b) Kim, S. S.; Park, M. H.; Chung, J. K.; Kim, W. J. *J. Appl. Phys.* **2009**, *105*, 061641.

(11) Melot, B. C.; Tacket, R.; O'Brien, J.; Hector, A. L.; Lawes, G.; Seshadri, R.; Ramirez, A. P. *Phys. Rev. B* **2009**, *79*, 224111.

(12) (a) Shoemaker, D. P.; Seshadri, R.; Hector, A. L.; Llobet, A.; Profen, T.; Fennie, C. J. *Phys. Rev. B* **2010**, *81*, 144113. (b) Shoemaker, D. P.; Seshadri, R.; Tachibana, M.; Hector, A. L. *Phys. Rev. B* **2011**, *84*, 064117.

(13) Seshadri, R. *Solid State Sci.* **2006**, *8*, 259.

(14) Henderson, S. J.; Shebanova, O.; Hector, A. L.; McMillan, P. F.; Weller, M. T. *Chem. Mater.* **2007**, *19*, 1712.

(15) Patterson, C. H. *Phys. Rev.* **2010**, *82*, 155103.

(16) Radosavljevic Evans, I.; Howard, J. A. K.; Evans, J. S. O. *J. Mater. Chem.* **2003**, *13*, 2098.

(17) Kennedy, B. J.; Ismunandar, Elcombe, M. M. *Mater. Sci. Forum* **1998**, *278–281*, 762.

(18) Jones, R. H.; Knight, K. S. *J. Chem. Soc., Dalton Trans.* **1997**, 2551.

(19) Mao, H.-K.; Xu, J.; Bell, P. M. *J. Geophys. Res.* **1986**, *91*, 4673.

(20) Liu, J.; Dubrovinsky, L.; Ballaran, T. B.; Crichton, W. *High Press. Res.* **2007**, *27*, 483.

(21) Hammersley, A. P.; Svensson, S. O.; Hanfland, M.; Fitch, A. N.; Hausermann, D. *High Press. Res.* **1996**, *14*, 235.

(22) Larson, A. C.; von Dreele, R. B. *General Structure Analysis System (GSAS)*. Los Alamos National Laboratory Report LAUR 86–748 2000; Toby, B. H. *J. Appl. Crystallogr.* **2001**, *34*, 210.

(23) Rodriguez-Carvajal, J. *Phys. B* **1993**, *55*, 192.

(24) Kraus, W.; Nolze, G. *J. Appl. Crystallogr.* **1996**, *29*, 301.

(25) Shirley, R. *Crysfire 2004*; University of Surrey, 2004.

(26) Scott, P. R.; Midgley, A.; Musaev, O.; Muthu, D. V. S.; Singh, S.; Suryanarayanan, R.; Revcolevski, A.; Sood, A. K.; Kruger, M. B. *High Press. Res.* **2011**, *31*, 219.

(27) (a) Cleave, A. R. Atomistic scale simulations for waste form analysis, PhD thesis, Imperial College, London, 2006. (b) Shevchenko, A. V.; Lopato, L. M. *Inorg. Mater.* **1982**, *18*, 1583. (c) Lopato, L. M.; Shevchenko, A. V.; Nazarenko, L. V. *Inorg. Mater.* **1984**, *20*, 1615.

(28) (a) Lian, J.; Wang, L.; Chen, J.; Sun, K.; Ewing, R. C.; Matt Farmer, J.; Boatner, L. A. *Acta Mater.* **2003**, *51*, 1493. (b) Begg, B. D.; Hess, N. J.; McCready, D. E.; Thevuthasan, S.; Weber, W. J. *J. Nucl. Mater.* **2001**, *289*, 188.

(29) Sorokina, S. L.; Sleight, A. W. *Mater. Res. Bull.* **1998**, *33*, 1077.

(30) Grey, I. E.; Roth, R. S. *J. Solid State Chem.* **200**, *150*, 167.

(31) Cai, L.; Nino, J. C. *Acta Crystallogr.* **2009**, *B65*, 269.

(32) McKie, D.; McKie, C. *Essentials of Crystallography*, 2nd ed.; Wiley-Blackwell, 1986; p 164.

(33) Webster, M. *Transform Unit Cell Program*; University of Southampton, 2002.

(34) Villars, P.; Calvert, L. D. *Pearson's Handbook of Crystallographic Data for Intermetallic Phases*, 2nd ed.; ASM International, Materials Park, OH, 1991.

(35) Navrotsky, A. *Geophys. Res. Lett.* **1980**, *7*, 709.